A Novel Approach to Modeling Coronary Stents Using a Slender Curved Rod Model: A Comparison Between Fractured Xience-like and Palmaz-like Stents

J. Tambača [*]   S. Čanić[†]   D. Paniagua, M.D.,[‡]

May 2, 2009

Abstract

We present a novel mathematical model to study the mechanical properties of endovascular stents in their expanded state. The model is based on the theory of slender curved rods. Stent struts are modeled as linearly elastic curved rods that satisfy the kinematic and dynamic contact conditions at the vertices where the struts meet. A weak formulation for the stent problem is defined and a Finite Element Method for a numerical computation of its solution is used to study mechanical properties of two commonly used coronary stents (Palmaz-like and Xience-like stent) in their expanded, fractured state. A simple fracture (separation), corresponding to one stent strut being disconnected from one vertex in a stent, was considered. Our results show a drastic difference in the response of the two stents to the physiologically reasonable uniform compression and bending forces.

Figure 1: Deployment of a coronary stent.

1 MOTIVATION

Mathematical and computer modeling of endovascular stents is an efficient way to improve their design and performance [1, 5, 6, 8, 9, 12, 14, 15, 16, 17, 22]. Currently available computational tools include "off the shelf," commercial software which is based on various three-dimensional Finite Element Method structure approximations of stent struts that form a three-dimensional stent mesh. Accurate, three-dimensional approximation of stents is often computationally very expensive in terms of time and memory requirements. This is why we developed a novel mathematical and computational algorithm which approximates three-dimensional stents as a **mesh of one-dimensional, elastic curved rods**.

Stent struts are modeled as linearly elastic, slender curved rods that satisfy the kinematic and dynamic contact conditions at the vertices where the struts meet. A weak formulation for the stent problem is defined and a Finite Element Method for a numerical computation of its solution was developed in [21]. The resulting FEM algorithm is incomparably simpler and faster than any corresponding three-dimensional solver, thereby enabling simulations of a large number of stent configurations in a short time.

Using this algorithm, we studied elastic deformation of stents **in their expanded state**, see Figure 2, exposed to physiologically reasonable pressure loads causing compression, expansion and bending. In particular, in this manuscript we compared the mechanical response to compression and bending of two commonly used coronary stents: a Palmaz-like stent and a Xience-like stent. Furthermore, a **fracture (separation)** was introduced prior to the computer simulations, corresponding to a separation of one stent strut from one vertex in the stent frame. Stent fractures and separation of coronary stent components are relatively rare (although fracture

2

of stents used in larger arteries such as those of the legs, are more common) but they cause potentially serious complications of coronary artery stenting [13, 18]. Patients whose coronary stents suffer from stent fracture may present non-specific symptoms of angina as a result of restenosis (re-narrowing of a coronary artery) or in-stent thrombosis, or both [13, 18]. In order to insure proper recognition and treatment of this problem, physicians must be aware of its existence and of the stent behavior under these circumstances [3]. In this manuscript we present a few scenarios that shed light on the mechanical behavior of two commonly used coronary stents under the assumption of a disconnection of one of the struts in the stent frame. New insights related to the performance of such coronary stents are obtained.

2   THE MODEL

We consider a stent to be a three-dimensional elastic body defined as a union of three-dimensional struts, see Figure 3 and Definition 1. The main
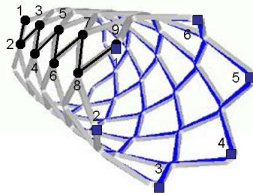

Figure 2: A stent with $n_C = 6$ and $n_L = 9$

novelty in this manuscript, over the standard approaches that can be found in literature [5, 22, 16, 6, 1, 9, 14, 15, 17, 12], is the use of the one-dimensional curved rod model to approximate the slender three-dimensional stent struts, and a definition of a stent as a union of curved rods satisfying certain contact conditions. The one-dimensional approximation is given in terms of the arc-length of the middle curve of the rod as an unknown variable. The cross-section of a rod representing each stent strut is assumed to be rectangular, of width w and thickness t. The curved stent struts "lie" on a cylinder with

3

reference (expanded) radius denoted by R, and reference (expanded) length denoted by L.

Struts themselves are assumed to be linearly elastic, with the elastic parameters given by the Lamé constants λ and μ, or, equivalently, by the Youngs modulus of elasticity E and the shear modulus μ.

2.1 Geometry: Parametrization of the Stent Frame

Without the loss of generality, we will be assuming that the stent struts form a uniform frame of diamonds with n_C vertices in the circumferential direction, and $n_L + 1$ vertices in the longitudinal direction, as shown in Figure 2. The assumption of uniform geometry is, however, not required for the implementation of the ideas described below, as they can be generalized to stents of arbitrary geometry with struts of different lengths. This will be utilized, for example, in Section 3.

Stent vertices will be denoted by $\boldsymbol{v}_{i,j}$, where $i = 1, \ldots, n_C$ and $j = 1, \ldots, n_L + 1$. See Figure 2. Vertices can be defined as

$$\boldsymbol{v}_{i,j} = (R\cos((i-1)\phi + (j-1)\phi/2), R\sin((i-1)\phi + (j-1)\phi/2), (j-1)\frac{L}{n_L})^T,$$

where $\phi = 2\pi/n_C$ is the angle formed by a vertex of a stent, the center of the circular cross-section of a stent, and an adjacent vertex on the same circumference of the stent, see Figure 3, left. The vertices on the adjacent
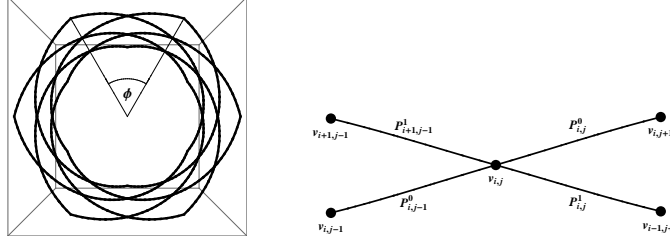

Figure 3: Left: The figure shows the angle formed by a vertex of a stent, the center of the circular cross-section, and an adjacent vertex on the stent. The angle is denoted by $\phi = 2\pi/n_C$. Right: The geometry of an interior vertex $\boldsymbol{v}_{i,j}$ with incoming and outgoing struts.

circular cross-section are shifted by the angle $\phi/2$. Each interior vertex is characterized by two incoming and two outgoing struts. See Figure 3, right.

Struts of a high precision laser cut stainless steel stent are not straight, but curved and located on the cylinder of radius R. To write the equations

4

for the curved stent struts we take a cord connecting the two vertices that define a strut, and then project the cord to the cylinder of radius R. See Figure 4. More precisely, denote by $R_{i,j}^k$, $k = 0, 1$, the two outgoing struts emerging from the vertex $\boldsymbol{v}_{i,j}$, and connecting to the vertices shifted by $\pm\phi/2$ at the level $j+1$. Then the cords (straight lines) corresponding to the struts $R_{i,j}^k$, $k = 0, 1$ can be parameterized as

$$
\begin{aligned}
S_{i,j}^k(s) &= s\boldsymbol{v}_{i,j} + (1-s)\boldsymbol{v}_{((i-1-k)\,\mathrm{mod}\,n_C)+1,j+1}, \quad s \in [0,1], \\
i &= 1, \ldots, n_C, \quad j = 1, \ldots, n_L, \quad k = 0, 1.
\end{aligned}
\tag{2.1}
$$

The *middle curve* of the curved stent struts $R_{i,j}^k$ can be expressed via the parameterization

$$
P_{i,j}^k : [0,1] \to \mathbb{R}^3,
$$

where

$$
P_{i,j}^k(s) = N S_{i,j}^k(s), \quad s \in [0,1], \ i = 1, \ldots, n_C, \ j = 1, \ldots, n_L, \ k = 0, 1. \tag{2.2}
$$

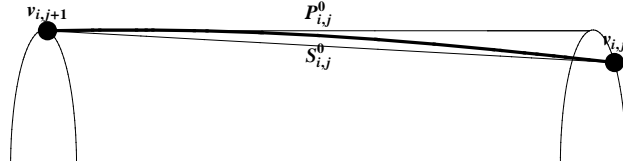Here N is the operator that lifts the cord up to the cylinder of radius R:

Figure 4: Curved stent strut.

$$
N\boldsymbol{v} = P\boldsymbol{v} + R\frac{\boldsymbol{v} - P\boldsymbol{v}}{\|\boldsymbol{v} - P\boldsymbol{v}\|},
$$

where P denotes the orthogonal projector on $\boldsymbol{e}_3$ in $\mathbb{R}^3$ with the standard scalar product, and $\{\boldsymbol{e}_1, \boldsymbol{e}_2, \boldsymbol{e}_3\}$ is the standard orthonormal basis of $\mathbb{R}^3$.

Using the parameterization $P_{i,j}^k$ of the middle curve of stent strut $R_{i,j}^k$ we can now introduce a parameterization of the *three-dimensional* stent strut $R_{i,j}^k$ as:

$$
\boldsymbol{\Phi}_{i,j}^k(s_1, s_2, s_3) = P_{i,j}^k(s_1) + s_2 \boldsymbol{n}_{i,j}^k(s) + s_3 \boldsymbol{b}_{i,j}^k(s), \tag{2.3}
$$

where $\boldsymbol{t}_{i,j}^k, \boldsymbol{n}_{i,j}^k$ and $\boldsymbol{b}_{i,j}^k(s)$ define a local basis at each point of the middle curve of stent strut $R_{i,j}^k$:

$$
\boldsymbol{t}_{i,j}^k(s) = \frac{(P_{i,j}^k)'(s)}{\|(P_{i,j}^k)'(s)\|}, \quad \boldsymbol{n}_{i,j}^k(s) = \frac{(I-P)P_{i,j}^k(s)}{\|(I-P)P_{i,j}^k(s)\|}, \quad \boldsymbol{b}_{i,j}^k(s) = \boldsymbol{t}_{i,j}^k(s) \times \boldsymbol{n}_{i,j}^k(s),
$$

5

for $s \in [0, 1]$. The parameterization $\mathbf{\Phi}_{i,j}^k$ maps the set $[0, 1] \times [-t/2, t/2] \times [-w/2, w/2]$ into $\mathbb{R}^3$.

Definition 1 *Three-dimensional stent Ω is a union of stent struts $R_{i,j}^k$ parameterized by $\mathbf{\Phi}_{i,j}^k$, given by (2.3):*

$$\Omega = \cup_{i=1}^{n_L} \cup_{j=1}^{n_C} \cup_{k=0}^1 \mathbf{\Phi}_{i,j}^k \text{ on } [0, 1] \times [-t/2, t/2] \times [-w/2, w/2]. \quad (2.4)$$

The interior stent surface of a stent is defined by

$$\Gamma_I = \cup_{i=1}^{n_L} \cup_{j=1}^{n_C} \cup_{k=0}^1 \mathbf{\Phi}_{i,j}^k \text{ on } [0, 1] \times \{-t/2\} \times [-w/2, w/2],$$

and the exterior stent surface by

$$\Gamma_E = \cup_{i=1}^{n_L} \cup_{j=1}^{n_C} \cup_{k=0}^1 \mathbf{\Phi}_{i,j}^k \text{ on } [0, 1] \times \{t/2\} \times [-w/2, w/2].$$

2.2 Mechanics: Stent as a Collection of Elastic Curved Rods

The curved rod model is a one-dimensional approximation of a three-dimensional rod-like structure to the ϵ^2 accuracy, where ϵ is the ratio between the largest dimension of the cross-section and the length of a rod. For a derivation and mathematical justification of the curved rod model see, e.g., [10] and [11]. In general, the behavior of a three-dimensional rod-like elastic body is approximated by the behavior of its middle curve and of its cross-sections. In the curved rod model, the cross-sections behave approximately as infinitesimal rigid bodies that remain perpendicular to the deformed middle curve.

More precisely, let $P : [0, \ell] \to \mathbb{R}^3$ be the natural parameterization of the middle curve of the rod of length ℓ ($\|P'(s)\| = 1, s \in [0, \ell]$). Then the curved rod model can be formulated as a first-order system of differential equations for the following unknown functions

- $\tilde{\boldsymbol{u}} : [0, \ell] \to \mathbb{R}^3$, the displacement of the middle curve of the rod;

- $\tilde{\boldsymbol{\omega}} : [0, \ell] \to \mathbb{R}^3$, the infinitesimal rotation of the cross-section of the rod;

- $\tilde{\boldsymbol{q}} : [0, \ell] \to \mathbb{R}^3$, the contact moment; and

- $\tilde{\boldsymbol{p}} : [0, \ell] \to \mathbb{R}^3$, the contact force.

(Here ℓ corresponds to the strut length, denoted by l_s.) For a given line force density $\tilde{\boldsymbol{f}}$, the equations of the curved rod model can be written as (see [19]):

$$\tilde{\boldsymbol{p}}' + \tilde{\boldsymbol{f}} = 0, \quad (2.1)$$
$$\tilde{\boldsymbol{q}}' + \boldsymbol{t} \times \tilde{\boldsymbol{p}} = 0, \quad (2.2)$$

describing the balance of contact force and contact moment, respectively, with

$$\tilde{\boldsymbol{\omega}}' - \mathbf{Q}\mathbf{H}^{-1}\tilde{\boldsymbol{Q}}^T\tilde{\boldsymbol{q}} = 0, \qquad (2.3)$$

$$\tilde{\boldsymbol{u}}' + \boldsymbol{t} \times \tilde{\boldsymbol{\omega}} = 0, \qquad (2.4)$$

describing the constitutive relations for a curved, linearly elastic rod. Here $\boldsymbol{t}$ is the unit tangent to the middle curve, $\mathbf{Q} = (\boldsymbol{t}, \boldsymbol{n}, \boldsymbol{b})$ is the orthogonal matrix containing the tangent vector $\boldsymbol{t}$ and vectors $\boldsymbol{n}$ and $\boldsymbol{b}$ that span the normal plane to the middle curve ($\mathbf{Q}$ describes the local basis at each point of the middle curve), and

$$\mathbf{H} = \begin{bmatrix} \mu K & 0 & 0 \\ 0 & EI_b & 0 \\ 0 & 0 & EI_n \end{bmatrix},$$

where $E = \mu\frac{3\lambda+2\mu}{\lambda+\mu}$ is the Young modulus of the material, I_n and I_b are moments of inertia of a cross-section and μK is the torsion rigidity of the cross-section. Therefore, $\mathbf{H}$ describes the elastic properties of the rod and the geometry of the cross-section.

Equation (2.4) is a condition that requires that the middle line is approximately inextensible and that allowable deformations of the cross-section are approximately orthogonal to the middle line. This condition has to be included in the solution space for the weak formulation of problem (2.1)-(2.4) (pure traction problem for a single curved rod). Thus, introduce the space

$$V = \left\{ (\tilde{\boldsymbol{v}}, \tilde{\boldsymbol{w}}) \in H^1(0,\ell)^6 : \tilde{\boldsymbol{v}}' + \boldsymbol{t} \times \tilde{\boldsymbol{w}} = 0 \right\}. \qquad (2.5)$$

Function $(\tilde{\boldsymbol{u}}, \tilde{\boldsymbol{\omega}}) \in V$ is called a weak solution of problem (2.1)-(2.4) if

$$\int_0^\ell \mathbf{QHQ}^T\tilde{\boldsymbol{\omega}}' \cdot \tilde{\boldsymbol{w}}' ds = \int_0^\ell \tilde{\boldsymbol{f}} \cdot \tilde{\boldsymbol{v}} ds + \tilde{\boldsymbol{q}}(\ell) \cdot \tilde{\boldsymbol{w}}(\ell) - \tilde{\boldsymbol{q}}(0) \cdot \tilde{\boldsymbol{w}}(0) + \tilde{\boldsymbol{p}}(\ell) \cdot \tilde{\boldsymbol{v}}(\ell) - \tilde{\boldsymbol{p}}(0) \cdot \tilde{\boldsymbol{v}}(0) \qquad (2.6)$$

holds for all $(\tilde{\boldsymbol{v}}, \tilde{\boldsymbol{w}}) \in V$ (notice the difference in the notation between $\tilde{\boldsymbol{\omega}}$ and $\tilde{\boldsymbol{w}}$).

To model the mechanical behavior of a stent as a **collection of one-dimensional** linearly elastic, homogeneous, isotropic curved rods, we parameterize the struts using the one-dimensional parameterizations $P_{i,j}^k$ of the struts' middle curves, see (2.2). Now a stent can be defined as a union of **one-dimensional** parameterizations as follows:

$$\Omega_1 = \bigcup_{i=1}^{n_C} \bigcup_{j=1}^{n_L} \bigcup_{k=0}^{1} P_{i,j}^k([0,1]).$$

Note that parameterizations $P_{i,j}^k$ are not arc-length parameterizations which is necessary for the formulation of the curved rod model (2.1)-(2.4). Nevertheless, they uniquely determine the middle curves of the stent struts and imply the existence of the arc-length parameterizations. Finding the arc-length parameterization in this case is a difficult task which is not necessary for the final formulation of the problem and the numerical method development.

Each of the curved rods approximating the stent struts $R_{i,j}^k$ satisfy a set of equations of the form (2.1)-(2.4). At the vertices where the curved rods meet, the kinematic and dynamic contact conditions determine the boundary condition for each curved rod in the stent frame structure. The kinematic contact condition describes the continuity of the kinematic quantities $\tilde{\boldsymbol{u}}_{i,j}^k$ and $\tilde{\boldsymbol{\omega}}_{i,j}^k$, stating that the displacement and the infinitesimal rotation for two struts meeting at a vertex, are the same. The dynamic contact condition is the equilibrium condition requiring that the sum of all contact forces at a vertex, and the sum of all contact moments at a vertex be equal zero. Thus,
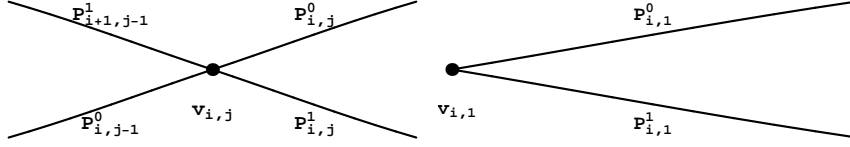

Figure 5: vertex $\boldsymbol{v}_{i,j}$

for each vertex $\boldsymbol{v}_{i,j}$ the kinematic contact conditions are given by

$$\tilde{\boldsymbol{u}}_{(i-1)\,\mathrm{mod}\,n_C+1,j-1}^0(l_s) = \tilde{\boldsymbol{u}}_{i\,\mathrm{mod}\,n_C+1,j-1}^1(l_s) = \tilde{\boldsymbol{u}}_{i,j}^0(0) = \tilde{\boldsymbol{u}}_{i,j}^1(0), \ (2.7)$$

$$\tilde{\boldsymbol{\omega}}_{(i-1)\,\mathrm{mod}\,n_C+1,j-1}^0(l_s) = \tilde{\boldsymbol{\omega}}_{i\,\mathrm{mod}\,n_C+1,j-1}^1(l_s) = \tilde{\boldsymbol{\omega}}_{i,j}^0(0) = \tilde{\boldsymbol{\omega}}_{i,j}^1(0), (2.8)$$

and the dynamic contact conditions are given by

$$\tilde{\boldsymbol{q}}_{(i-1)\,\mathrm{mod}\,n_C+1,j-1}^0(l_s) + \tilde{\boldsymbol{q}}_{i\,\mathrm{mod}\,n_C+1,j-1}^1(l_s) + \tilde{\boldsymbol{q}}_{i,j}^0(0) + \tilde{\boldsymbol{q}}_{i,j}^1(0) = 0, \ (2.9)$$

$$\tilde{\boldsymbol{p}}_{(i-1)\,\mathrm{mod}\,n_C+1,j-1}^0(l_s) + \tilde{\boldsymbol{p}}_{i\,\mathrm{mod}\,n_C+1,j-1}^1(l_s) + \tilde{\boldsymbol{p}}_{i,j}^0(0) + \tilde{\boldsymbol{p}}_{i,j}^1(0) = 0,(2.10)$$

for $i = 1, \ldots, n_C, j = 1, \ldots, n_L + 1$ with the convention that the quantity is removed for nonexistent indexes corresponding to the end vertices $\boldsymbol{v}_{i,1}$ and $\boldsymbol{v}_{i,n_L+1}$.

To define a weak formulation for the stent frame problem introduce the following function space:

$$V_F = \left\{ (\tilde{\boldsymbol{v}}_{1,1}^0, \tilde{\boldsymbol{w}}_{1,1}^0, \ldots, \tilde{\boldsymbol{v}}_{n_C,n_L}^1, \tilde{\boldsymbol{w}}_{n_C,n_L}^1) : (\tilde{\boldsymbol{v}}_{i,j}^k, \tilde{\boldsymbol{w}}_{i,j}^k) \in V_{i,j}^k \ \& \ (2.7), (2.8) \ \mathrm{hold} \right\},$$

8

where $V_{i,j}^k$ are the function spaces (2.5) corresponding to the struts $R_{i,j}^k$.

Now the **weak formulation for the stent frame structure consisting of curved rods** is given by the following:

Definition 2 *Function $(\tilde{\boldsymbol{u}}_{1,1}^0, \tilde{\boldsymbol{\omega}}_{1,1}^0, \ldots, \tilde{\boldsymbol{u}}_{n_C,n_L}^1, \tilde{\boldsymbol{\omega}}_{n_C,n_L}^1) \in V_F$ is a weak solution to the stent frame problem if*

$$\sum_{i=1}^{n_C} \sum_{j=1}^{n_L} \sum_{k=0,1} \int_0^{l_s} \mathbf{Q}_{i,j}^k \mathbf{H} (\mathbf{Q}_{i,j}^k)^T (\tilde{\boldsymbol{\omega}}_{i,j}^k)' \cdot (\tilde{\boldsymbol{w}}_{i,j}^k)' ds = \int_0^{l_s} \tilde{\boldsymbol{f}}_{i,j}^k \cdot \tilde{\boldsymbol{v}}_{i,j}^k ds \quad (2.11)$$

holds for all $(\tilde{\boldsymbol{v}}_{1,1}^0, \tilde{\boldsymbol{w}}_{1,1}^0, \ldots, \tilde{\boldsymbol{v}}_{n_C,n_L}^1, \tilde{\boldsymbol{w}}_{n_C,n_L}^1) \in V_F$.

Notice again the difference in the notation for the infinitesimal rotation test functions $\tilde{\boldsymbol{w}}_{i,j}^k$ and the notation for the infinitesimal rotation solution functions $\tilde{\boldsymbol{\omega}}_{i,j}^k$. Also notice that all the intermediate boundary terms on the right hand-side of equation (2.6) cancel out in the formulation (2.11) due to the kinematic and dynamics contact conditions.

Solution to problem (2.11) is not unique. Namely, since only the derivative of $\tilde{\boldsymbol{\omega}}$ appears in the weak formulation, the solution will be determined up to a constant $\tilde{\boldsymbol{\omega}}_0$. Thus, if P is a point on the frame structure, then $\tilde{\boldsymbol{\omega}}(P) = \tilde{\boldsymbol{\omega}}_0$ is in the kernel of the problem. Furthermore, from the condition $\tilde{\boldsymbol{u}}' + \boldsymbol{t} \times \tilde{\boldsymbol{\omega}} = 0$, with $\tilde{\boldsymbol{\omega}}$ constant, one can solve the equation for $\tilde{\boldsymbol{u}}$ to obtain $\tilde{\boldsymbol{u}}(s) = \tilde{\boldsymbol{u}}_0 - P \times \tilde{\boldsymbol{\omega}}_0 = \tilde{\boldsymbol{u}}_0 + \tilde{\boldsymbol{\omega}}_0 \times P$. Thus, the infinitesimal rotation of the cross-section and displacement of P are unique up to the term

$$\left[\begin{array}{c} \tilde{\boldsymbol{\omega}}(P) \\ \tilde{\boldsymbol{u}}(P) \end{array} \right] = \left[\begin{array}{c} \tilde{\boldsymbol{\omega}}_0 \\ \tilde{\boldsymbol{u}}_0 + \tilde{\boldsymbol{\omega}}_0 \times P \end{array} \right],$$

for arbitrary vectors $\tilde{\boldsymbol{u}}_0, \tilde{\boldsymbol{\omega}}_0 \in \mathbb{R}^3$. This means that the solution is unique up to the translation and infinitesimal rotation of the frame structure. Thus we will be interested in the solution of (2.11) that satisfies an additional condition

$$\int_F \tilde{\boldsymbol{u}}(P) \cdot (\boldsymbol{a} + \boldsymbol{b} \times P) dP = 0, \quad \forall \boldsymbol{a}, \boldsymbol{b} \in \mathbb{R}^3. \quad (2.12)$$

2.3 Numerical Implementation

The frame structure presented in this section is still extremely complex. The main obstacle for the numerical treatment of the problem of the form (2.11) is the implementation of the condition in the function spaces $V_{i,j}^k$ that should be satisfied by the test functions. For this reason, we made a further simplification that incorporates approximation of each curved rod by

the piecewise straight rods. This approximation has been mathematically justified in [19] and [20]. For details, please see [21]. A Finite Element Method was developed in [21] for a solution to this problem. Numerical results are presented next.

3 NUMERICAL RESULTS

The mechanical behavior of two types of stents is considered below: a Xience-like stent (nonuniform geometry) shown in Figure 6, and a Palmaz-like stent (uniform geometry), shown in Figure 14. Both stents are subject to two loading scenarios: uniform compression and bending.

Uniform compression: A uniformly distributed force in the radial direction is applied to stents causing compression. Radial displacement from the expanded configuration is measured. The compression force corresponds to the pressure load of 0.5 atmospheres. The force is calculated by considering the 0.5 atm pressure load of a *cylinder* (e.g., blood vessel) of length L acting on a *stent* of the same length L. This pressure load is physiologically reasonable. Namely, we can use the Law of Laplace to estimate exterior pressure loads to an inserted stent. Recall that the Law of Laplace relates the displacement u of the arterial wall with the transmurral pressure $p - p_0$, [7], via:

$$p - p_0 = \frac{Eh}{(1 - \nu^2)R^2} u, \tag{3.13}$$

where E is the Youngs modulus of the vessel wall, h is the vessel wall thickness, R the vessel (reference) radius and ν the Poisson ratio. For incompressible materials such as arterial walls (nearly compressible), $\nu = 1/2$. The Youngs modulus of a coronary artery is between 10^5Pa and 10^6Pa, see e.g., [2] and the references therein. For our calculation let us take the intermediate value of $E = 5 \times 10^5$ Pa, and let us take the reference coronary artery radius to be around 1.3mm with the vessel wall thickness $h = 1$mm. Stents are typically oversized by 10% of the native vessel radius to provide reasonable fixation. Thus, 10% displacement of a coronary artery of radius 1.3mm is 0.13mm. This gives $u = 0.13$mm. By plugging these values into formula (3.13) one gets $p - p_0 \approx 5 \times 10^4$Pa which equals 0.5 atm. Thus, a pressure load of 0.5 atm is necessary to expand a coronary artery by 10% of its reference radius. This force is applied to the stents studied below to capture the stent deformation under the coronary artery loading.

Bending: In the examples below we will be calculating stent deformation to forces causing bending. These forces will be applied pointwise to the

center of a given stent (at 2-4 points in the center) and to the end points (at 1 point near each end of a stent). The force at the end points is applied in the opposite direction from the force applied to the center of the stent. The magnitude of the total applied force is calculated for each stents to be equal to the force that a curved vessel, with the radius of curvature $R_c = 2.5cm$, exerts on a straight stent that is inserted into the curved vessel. Stents with higher bending rigidity will deform less, while stents with low bending rigidity will deform more.

3.1 Xience-like Stent (Stent X) (Non-uniform geometry)

The stent geometry is that of Multi-Link Mini Vision, resembling Xience stent by Abbott shown in Figure 6, left. Figure 6 right shows our computer-generated geometry of a Xience-like stent. The stent struts are made of Cobalt Chromium (CoCr) (L-605) (CoCr, Young's modulus $E = 2.43 \times 10^{11} Pa$) with thickness $0.08mm$. Stent struts are organized in zig-zag rings ("in-phase" rings) connected with horizontal struts which contain one wiggle near the protruding vertex of a zig-zag ring. Stent X has $n_C = 6$ vertices in the circumferential direction and $n_L = 24$ vertices in the longitudinal direction with reference radius $R = 1.5mm$.

Figure 6: Xience stent by Abbott (left); Computationally generated Xience-like stent (right) showing half of the mesh with $n_C = 6$ and $n_L = 24$.

In the examples below a fractured Xience-like stent will be considered, with a fracture corresponding to a disconnection of one strut from one vertex. In particular, a vertex in the middle of the stent is chosen to suffer component separation, see Figures 7, 12. Namely, our simulations show that this vertex suffers from highest contact moments during bending (and compression). Denote this vertex by $\tilde{\mathbf{v}}$. There are three struts that meet at vertex $\tilde{\mathbf{v}}$: two symmetric, diagonally placed ones forming one zig-zag geometry in the zig-zag ring of stent struts, see Figure 7 bottom, and one horizontally placed strut connecting two different zig-zag rings, see Figure 12. We will consider below two examples: the first is an example of a Xience-like stent with a separated diagonally placed strut, and the second is an example of a Xience-like stent with a separated horizontally placed strut.
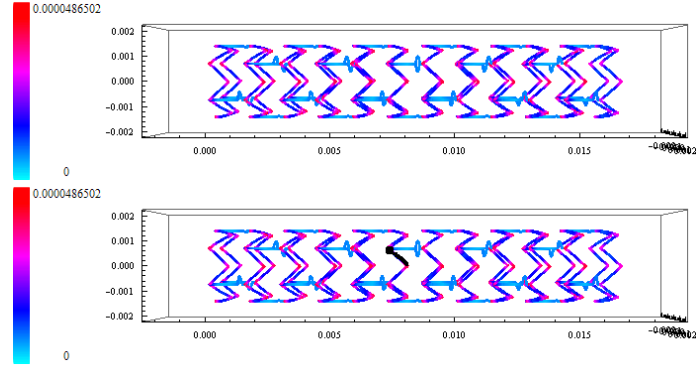
11

Figure 7: Non-fractured Xience-like stent exposed to uniform compression. Stent struts are colored based on the magnitude of contact moment. The bottom figure shows the strut which will be disconnected from vertex $\tilde{\mathbf{v}}$, colored with a black dot.
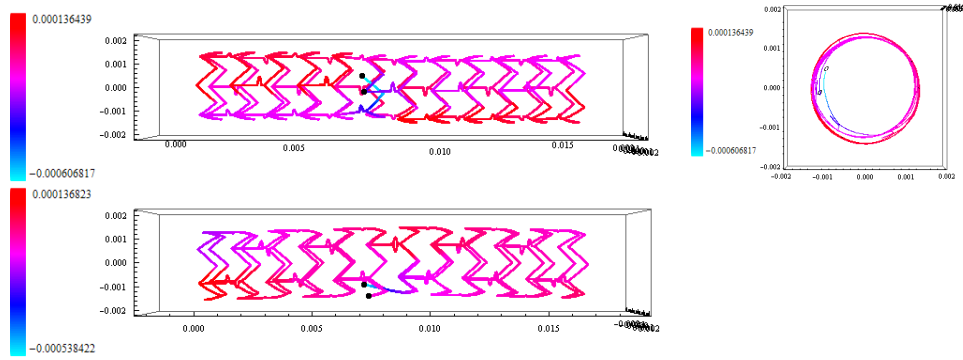

Figure 8: Fractured Xience-like stent under uniform pressure load (3 different views). The dislocated stent strut is shown in blue (cyan). The dots on the figure denote the points corresponding to the fractured vertex of a stent where the dislocated strut was broken away from the reference stent frame. The stent is colored based on the magnitude of the radial displacement.
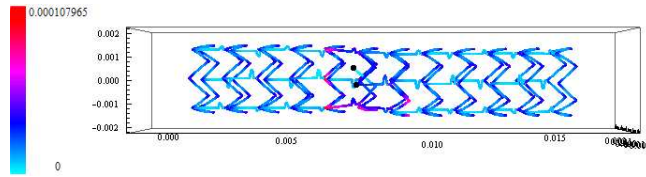

Figure 9: Fractured Xience-like stent from Figure 8 under uniform pressure load. The stent is colored based on the magnitude of the contact moment.
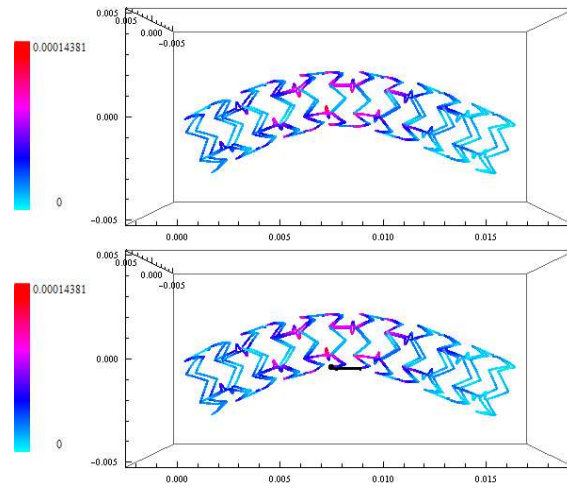
12

Figure 10: Non-fractured Xience-like stent exposed to bending forces. Stent struts are colored based on the magnitude of the contact moment. The strut shown in black (right figure) denotes the strut that will be disconnected from the vertex denoted with a black dot.
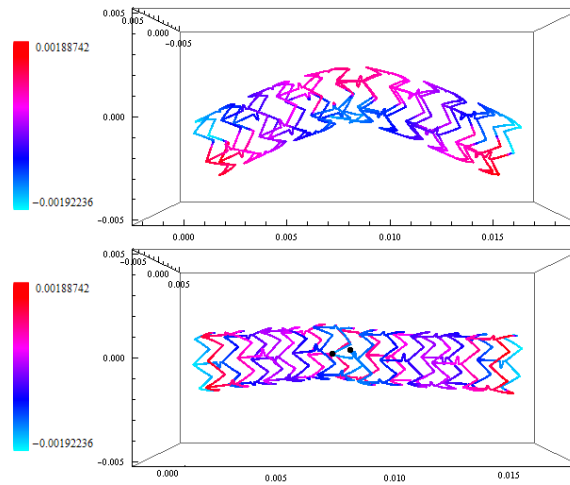

Figure 11: Fractured Xience-like stent exposed to bending forces. Stent struts are colored based on the magnitude of the radial displacement. Two views are shown: a side view (top) and a view from the bottom of the deformed stent (bottom).

13

Example 1. Xience-like stent with a disconnected diagonally placed strut emerging from vertex $\tilde{\mathbf{v}}$ is exposed to uniform compression and bending. Figure 7 shows the bending moments for a non-fractured Xience-like stent, with a strut that is to be disconnected from vertex $\tilde{\mathbf{v}}$ shown in black. Figure 8 shows radial displacement under uniform compression of the fractured stent. The disconnected strut is shown in light blue (cyan). The two views show that the strut disconnected from vertex $\tilde{\mathbf{v}}$ protrudes into the lumen of the stented vessel by around 30% of the reference radius, causing potential for complications associated with in-stent thrombosis, as observed in clinical practice [13].

Figure 9 shows that the deformation of the disconnected strut causes higher contact moments. A comparison between the numbers on the scale shown on the left in Figures 7 and 9 indicate that the maximum bending moment for the deformed stent with a disconnected diagonally placed strut is two times the contact moment of a non-fractured stent exposed to uniform compression. This is a precursor for possible further stent fractures that may be associated with this highly flexible and compliant stent.

Bending: Figure 10 shows contact moments for Xience-like stent exposed to bending forces. The bottom figure indicates the strut that is to be disconnected from vertex $\tilde{\mathbf{v}}$ (shown in black). The result of the bending load applied to the Xience-like stent with a disconnected diagonally placed strut is shown in Figure 11. The stent bends more than the non-fractured one. The calculated bending factors (reciprocal of the radius of curvature) for the non-fractured Xience-like stent (Stent X) and the fractured Xience-like stent (Stent X-frac1) are shown in Figure 19. Figure 11 top shows the stent from the side view, and the bottom figure shows the same stent from the bottom view. The two black dots denote the disconnected vertex, viewed from below of the curved stent.
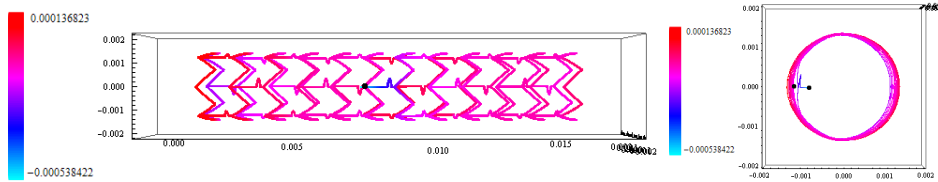

Figure 12: Fractured Xience-like stent under uniform pressure load. Stent struts are colored based on the magnitude of the radial displacement. The circles on the figure denote the points corresponding to the fractured vertex of a stent. The disconnected strut, shown in blue, protrudes into the lumen with the largest radial displacement of all the struts.
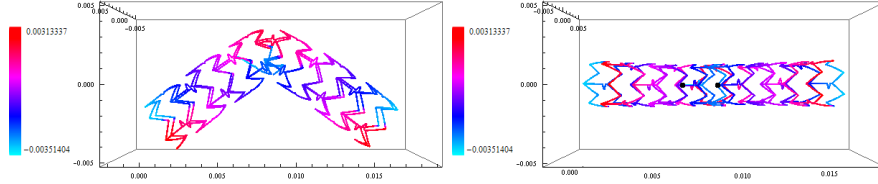
Figure 13: Bending of a fractured Xience-like stent. Struts are colored based on the magnitude of the radial displacement. Two views are shown: a side view (left) and a view from the bottom of the stent (right). Catastophic deformation is observed.

Example 2. Xience-like stent with a disconnected horizontally placed strut emerging from vertex $\tilde{\mathbf{v}}$ is exposed to uniform compression and bending. Figure 8 shows radial displacement under uniform compression of the fractured stent (the magnitude of the radial displacement is shown in the scale bar on the left of the figure). The disconnected strut is shown in light blue (cyan). The two views show that the disconnected strut protrudes into the lumen of the stented vessel causing potential for complications associated with thrombosis.

Bending: Figure 13 shows a catastrophic deformation of a Xience-like stent with a disconnected horizontal strut under bending load. The disconnected strut is placed at the bottom, at the center of the bent stent. Figure 13 shows two views of the stent: the side view and the view from the bottom where the center of curvature of the bent stent lies. This deformation is too large for the model presented in this paper to be used to calculate accurate displacement and/or moments of the deformed stent. Our simulation, however, indicates that a disconnection of a central horizontal strut in a Xience-like stent will likely lead to unacceptable deformation under bending forces.

3.2   Palmaz-like Stent (Stent P) (Uniform geometry)

A Palmaz-like stainless steel stent (316L) such as the one shown in Figure 14, with uniform geometry containing $n_C = 6$ vertices in the circumferential direction and $n_L = 24$ vertices in the longitudinal (axial) direction is considered. The stent has been expanded to the radius of $1.5mm$ into its reference configuration.

Figure 15 shows contact moments and radial displacement of a Palmaz-like stent under uniform compression. This stent deforms more at the end points (radial displacement shown in light blue) than at the center (radial

Figure 14: A photograph of Palmaz stent by Cordis.

displacement shown in red). One of the diagonally placed struts was disconnected from a vertex $\tilde{\mathbf{v}}$ at the "center" of the stent, shown in Figure 16 with a black dot.
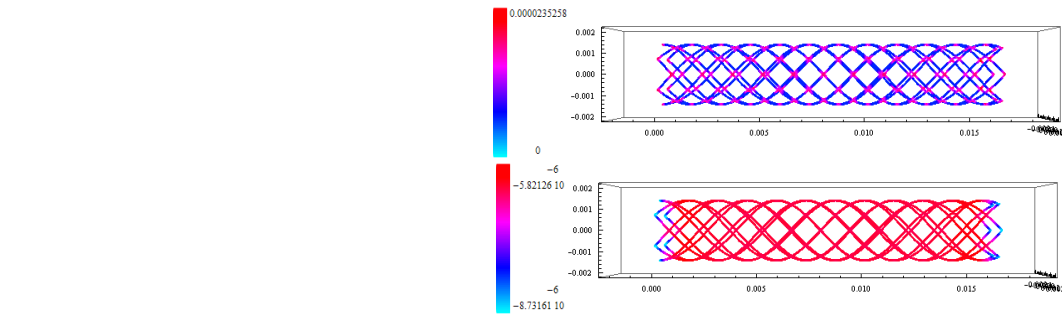

Figure 15: Non-fractured Palmaz-like stent under uniform compression. Stent struts are colored based on the magnitude of contact moments (top) and radial displacement (bottom). Negligible radial displacement is observed.

We see that, although the disconnected strut deforms more than the neighboring struts (shown in light blue versus red in Figure 16), the deformation is 25 times smaller (2×10^{-5} meters versus 5×10^{-4} meters) than the deformation of the Xience-like stent with an "equivalent" disconnected strut shown in Figure 8. Thus, we conclude that a Palmaz-like stent with a disconnected strut in the center of a stent deforms less under uniform compression than a Xience-like stent with an equivalent disconnected strut (diagonally placed), see Figure 8.

Bending: In the reminder of this section we study the behavior of a fractured Palmaz-like stent under bending forces. Figure 17 shows the magnitude
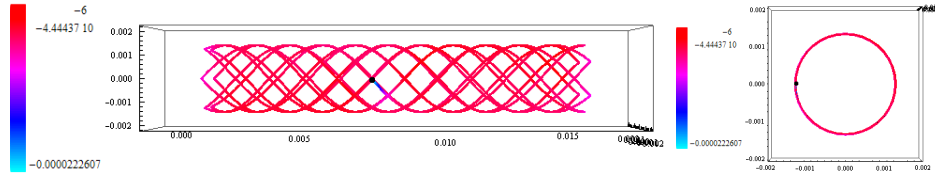
16

Figure 16: Fractured Palmaz-like stent under uniform compression. Struts are colored based on the magnitude of radial displacement. The disconnected strut is shown in blue, with the black dot denoting the vertex from which the strut is disconnected. Two views are shown: a side view (left) and an axial view (right). The displacement of the disconnect strut is only 0.5% of the reference configuration.

of the contact moment under the same bending forces as those that were applied to the Xience-like stent, shown in Figure 10. It is obvious that Palmaz-like stents have much higher bending rigidity than Xience-like stents. Figure 18 shows the magnitude of the contact moment for a Palmaz-like stent
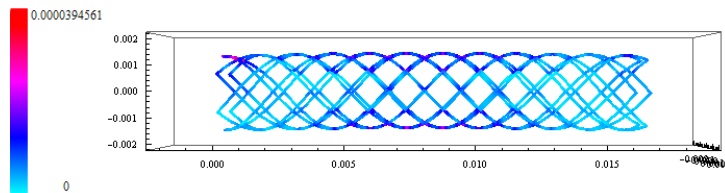

Figure 17: Non-fractured Palmaz-like stent exposed to bending forces. Same bending forces are use as those corresponding to Figure 10. Stent struts are colored based on the magnitude of contact moment. Much smalled bending can be observed in comparison with the bending of a non-fractured Xience-like stent, shown in Figure 10.

under bending forces with a disconnected strut from the vertex, shown in Figure 18 with a black dot. Very small difference between the behavior of a non-fractured stent shown in Figure 17 and a fractured Palmaz-like stent shown in Figure 18 is observed.

4   Conclusions

Our model, based on the approximation of a three-dimensional stent strut mesh as a collection of slender curved rods, enables fast and accurate simulation of mechanical behavior of stents in their expanded state [21]. We
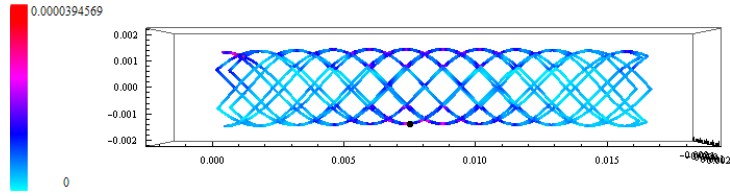
17

Figure 18: Fractured Palmaz-like stent exposed to bending forces. Stent struts are colored based on the magnitude of contact moment. The black dot denotes the vertex from which a diagonally placed strut was disconnected. Much smaller bending can be observed in comparison with the bending of a fractured Xience-like stent shown in Figure 11.
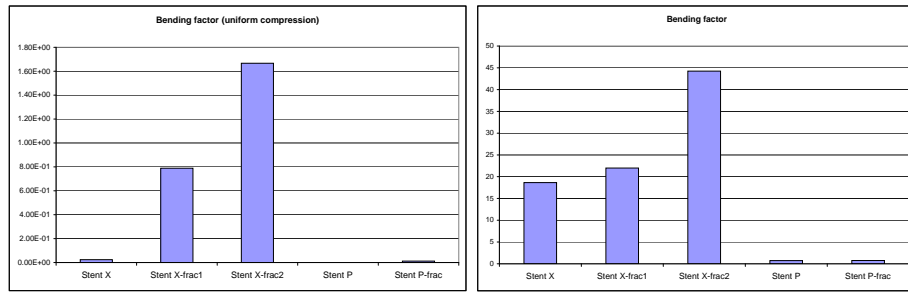

Figure 19: Graphs showing the bending factor for the five stents: non-fractured Xience-like stent (stent X), fractured Xience-like stent from Example 1 (stent X-frac1), fractured Xience-like stent from Example 2 (stent X-frac2), non-fractured Palmaz-like stent (stent P) and fractured Palmaz-like stent (stent P-frac). Bending factor is calculated as the reciprocal of the radius of curvature for each deformed stent. Left:: stents were exposed to the same uniform compression forces, as described at the beginning of Section 3. Right: stents were exposed to the same bending forces, as described at the beginning of Section 3.

18

used this model to study deformation of Palmaz-like stent and Xience-like stent with a fracture introduced prior to the simulation. The stent fractures considered in this manuscript correspond to a disconnection of one stent strut from one vertex. Drastic differences between the mechanical responses to uniform compression and bending of the Xience-like stent and of the Palmaz-like stent were detected. The following conclusions were obtained:

1. Palmaz-like stent is much stiffer than the Xience-like stent both under uniform compression and under bending force (compare Figures 7 and 15, and Figures 10 and 17). This, in turn, implies less deformation of a fractured Palmaz-like stent, see Figure 16, than the Xience-like stent, see Figure 8, and the overall smaller contact moments in the Palmaz-like stent introduced by a disconnection of a strut from the stent frame.

2. Disconnection of a horizontally placed strut in a Xience-like stent may lead to catastrophic deformation when such a stent is located in the tortuous (curved) geometry, which is the typical application of Xience-like stents, where the stent is naturally exposed to bending forces. See Figure 11.

3. Disconnection of any one strut in a Xience-like stent causes protrusion of a stent strut into the lumen of a stented artery by around 30% of its expanded radius, providing an environment that promotes coronary in-stent thrombosis and in-stent restenosis as clinicaly observed in [13, 18]. See Figure 8.

4. Disconnection of a diagonally-placed strut in a Xience-like stent causes visible bending of the stent even when the stent is exposed to uniform compression forces. See Figure 8 bottom and graphs in Figure 19 left.

5. Deformation of a fractured Xience-like stent (with one strut separated from one vertex) is significantly larger than the deformation of a fractured Palmaz-like stent when exposed to uniform compression during arterial pulsation and bending.

References

[1] J.L. Berry, A. Santamarina, J.E. Moore Jr., S. Roychowdhury, and W.D. Routh. *Experimental and Computational Flow Evaluation of Coronary Stents* Annal of Biomedical Engineering 28 (2000) 386–398.

[2] S. Canic, C.J. Hartley, D. Rosenstrauch, J. Tambaca, G. Guidoboni, A. Mikelic. *Blood Flow in Compliant Arteries: An Effective Viscoelastic Reduced Model, Numerics and Experimental Validation.* Annals of Biomedical Engineering. 34 (2006) 575 - 592.

[3] A. Carter. Stent strut fracture: Seeing is believing. Cathet Cardiovasc Interv 71 (2008) 619-620.

[4] P.G. Ciarlet, Mathematical Elasticity. Volume I: Three-Dimensional Elasticity, North-Holland, Amsterdam, 1988.

[5] C. Dumoulin and B. Cochelin. *Mechanical behavior modeling of balloon-expandable stents* Journal of Biomechanics 33(11) (2000) 1461–1470.

[6] A.O. Frank, P.w. Walsh and J.E. Moore Jr. *Computational Fluid Dynamics and Stent Design* Artificial Organs 26(7) (2002) 614–621.

[7] Y.C. Fung *Biomechanics: Mechanical Properties of Living Tissues.* Second Edition. Springer 1993.

[8] G. Hausdorf. *Mechanical and Biophysical Aspects of Stents,*in *Catheter Based Devices for the Treatment of Non-coronary Cardiovascular Diseases in Adults and Children.* Ed. P. Syamasundar Rao and Morton J. Kern. Lippincott Williams & Wilkins, Philadelphia 2003.

[9] V. Hoang, *Stent Design and Engineered Coating Over Flow Removal Tool*, Team #3 (Vimage), 10/29/04.

[10] M. Jurak, J. Tambača, *Derivation and justification of a curved rod model*, Mathematical Models and Methods in Applied Sciences 9 (1999) 7, 991–1014.

[11] M. Jurak, J. Tambača, *Linear curved rod model. General curve*, Mathematical Models and Methods in Applied Sciences 11 (2001) 7, 1237–1252.

[12] KW Lau, A. Johan, U. Sigwart, JS Hung, *A stent is not just a stent: stent construction and design do matter in its clinical performance*, Singapore Medical Journal **45** (2004) 7, 305–312.

[13] A. N. Makaryusm, L. Lefkowitz and A. D. K. Lee, Coronary artery stent fracture. Int J Cardiovasc Imaging 23 (2007) 305–309.

[14] McClean Dougal R, MD, Eigler N, MD, *Stent Design: Implications for Restenosis*, MedReviews, LLC 2002.

[15] F. Migliavacca, L. Petrini, M. Colombo, F. Auricchio, R. Pietrabissa. *Mechanical behavior of coronary stents investigated through the finite element method* Jurnal of Biomechanics 35 (2002) 803–811.

[16] J.E. Moore Jr. and J.L. Berry. *Fluid and Solid Mechanical Implications of Vascular Stenting.* Annals of Biomedical Engineering 30 (2002) 498–508.

[17] A.C. Morton, D. Crossman, J. Gunn., *The influence of physical stent parameters upon restenosis*, Pathologie Biologie **52** (2004) 196–205.

[18] F. Shaikh, R. Maddikunta, M Djelmami-Hani, J. Solis, S. Allaqaband, and T. Bajwa. Stent fracture, an incidental finding or a significant marker of clinical in-stent restenosis. Cathet Cardiovasc Interv 71 (2008) 614-618.

[19] J. Tambača, *A model of irregular curved rods*, in Proceedings of the Conference on Applied Mathematics and Scientific Computing (Dubrovnik, 2001), eds. Z. Drmač, V. Hari, L. Sopta, Z. Tutek, K. Veselić, Kluwer, 2003, 289–299.

[20] J. Tambača, *A numerical method for solving the curved rod model*, ZAMM **86** (2006), 210–221.

[21] J. Tambača, M. Kosor, S. Čanić, D. Paniagua. Mathematical Modeling of Vascular Stents. SIAM J Appl. Math. Under revision.

[22] L.H. Timmins, M.R. Moreno, C.A. Meyer, J.C. Criscione, A. Rachev and J.E. Moore Jr. *Stented artery biomechanics and device design optimization.* Med. Bio. Eng. Comput 45 (2007) 505–513.